A TCR β-Chain Motif Biases toward Recognition of Human CD1 Proteins

Peter Reinink, Adam Shahine, Stephanie Gras, Tan-Yun Cheng, Rachel Farquhar, Kattya Lopez, Sara A. Suliman, Josephine F. Reijneveld, Jérôme Le Nours, Li Lynn Tan, Segundo R. León, Judith Jimenez, Roger Calderon, Leonid Lecca, Megan B. Murray, Jamie Rossjohn, D. Branch Moody and Ildiko Van Rhijn

Supplementary Material	http://www.jimmunol.org/content/suppl/2019/11/05/jimmunol.1900872.DCSupplemental
References	This article **cites 67 articles**, 28 of which you can access for free at: http://www.jimmunol.org/content/203/12/3395.full#ref-list-1

Why *The JI*? Submit online.

- **Rapid Reviews! 30 days*** from submission to initial decision

- **No Triage!** Every submission reviewed by practicing scientists

- **Fast Publication!** 4 weeks from acceptance to publication

*average

Subscription	Information about subscribing to *The Journal of Immunology* is online at: http://jimmunol.org/subscription
Permissions	Submit copyright permission requests at: http://www.aai.org/About/Publications/JI/copyright.html
Email Alerts	Receive free email-alerts when new articles cite this article. Sign up at: http://jimmunol.org/alerts

A TCR β-Chain Motif Biases toward Recognition of Human CD1 Proteins

Peter Reinink,*[,†,1] Adam Shahine,[‡,§,1] Stephanie Gras,[‡,§] Tan-Yun Cheng,[†]
Rachel Farquhar,[‡,§] Kattya Lopez,[†,¶] Sara A. Suliman,[†] Josephine F. Reijneveld,*[,†,∥]
Jérôme Le Nours,[‡,§] Li Lynn Tan,[‡,§] Segundo R. León,[¶] Judith Jimenez,[¶]
Roger Calderon,[¶] Leonid Lecca,[¶] Megan B. Murray,[#,**,††] Jamie Rossjohn,[‡,§,‡‡]
D. Branch Moody,[†] and Ildiko Van Rhijn*[,†]

High-throughput TCR sequencing allows interrogation of the human TCR repertoire, potentially connecting TCR sequences to antigenic targets. Unlike the highly polymorphic MHC proteins, monomorphic Ag-presenting molecules such as MR1, CD1d, and CD1b present Ags to T cells with species-wide TCR motifs. CD1b tetramer studies and a survey of the 27 published CD1b-restricted TCRs demonstrated a TCR motif in humans defined by the TCR β-chain variable gene 4-1 (TRBV4-1) region. Unexpectedly, TRBV4-1 was involved in recognition of CD1b regardless of the chemical class of the carried lipid. Crystal structures of two CD1b-specific TRBV4-1[+] TCRs show that germline-encoded residues in CDR1 and CDR3 regions of TRBV4-1–encoded sequences interact with each other and consolidate the surface of the TCR. Mutational studies identified a key positively charged residue in TRBV4-1 and a key negatively charged residue in CD1b that is shared with CD1c, which is also recognized by TRBV4-1 TCRs. These data show that one TCR V region can mediate a mechanism of recognition of two related monomorphic Ag-presenting molecules that does not rely on a defined lipid Ag. *The Journal of Immunology*, 2019, 203: 3395–3406.

M ajor histocompatibility complex–encoded Ag-presenting molecules and the structurally related CD1 and MR1 molecules all present Ags to αβ T cells. In humans, the CD1 family consists of four cell surface–expressed Ag-presenting molecules, CD1a, CD1b, CD1c, and CD1d, that present lipids to T cells (1). Whereas MHC, CD1, and MR1 proteins all display chemically diverse Ags, a major difference among them involves genetic diversity. Whereas the human *MHC* locus shows the highest rates of polymorphism among genomes, polymorphisms in the coding regions of *CD1* and *MR1* are rare. The few single-nucleotide polymorphisms in *CD1* genes are not known to control Ag presentation, suggesting that CD1 proteins are functionally equivalent among most or all humans (2, 3). These marked differences in the interindividual variability of MHC, MR1, and CD1 Ag-presenting molecules, together with their distinct structural features, potentially translate into differing patterns of αβ TCRs controlled by these systems.

Based on more than 100 solved MHC–peptide–TCR structures (4–7), docking of TCRs on MHC is well understood in general terms. First, the V domains of the α-chain and β-chain are positioned over the α2 helix and α1 helix of MHC class I, respectively. Second, V gene–encoded CDR1 or CDR2 frequently interacts with the outer α helices of MHC molecules. Despite notable exceptions (8, 9), this general structural model might predict that certain MHC types or allomorphs preferentially interact with certain V gene–encoded segments and that MHC haplotype biases the selected TCR repertoire in ways that can be specifically detected by sequencing of the TCR repertoire. However, there is only limited data available to support this concept, and the existing data only account for a minor association between MHC haplotype and TCR gene bias (10). The alternative hypothesis is that population-based genetic diversity in the MHC system, the diversity of the bound peptides for any allomorph, and the fact that each MHC molecule or allomorph can interact with many

---

*Department of Infectious Diseases and Immunology, Faculty of Veterinary Medicine, Utrecht University, 3584CL Utrecht, the Netherlands; †Division of Rheumatology, Inflammation, and Immunity, Brigham and Women's Hospital and Harvard Medical School, Boston, MA 02115; ‡Infection and Immunity Program and Department of Biochemistry and Molecular Biology, Biomedicine Discovery Institute, Monash University, Clayton, Victoria 3800, Australia; §Australian Research Council Centre of Excellence in Advanced Molecular Imaging, Monash University, Clayton, Victoria 3800, Australia; ¶Socios en Salud Sucursal Peru, 15001 Lima, Peru; ∥Stratingh Institute for Chemistry, University of Groningen, 9747AG Groningen, the Netherlands; #Department of Global Health and Social Medicine, Harvard Medical School, Boston, MA 02115; **Division of Global Health Equity, Brigham and Women's Hospital, Boston, MA 02115; ††Department of Epidemiology, Harvard School of Public Health, Boston, MA 02115; and ‡‡Institute of Infection and Immunity, School of Medicine, Cardiff University, CF14 4XN Cardiff, United Kingdom

[1]P.R. and A.S. contributed equally.

ORCIDs: 0000-0002-9836-1335 (P.R.); 0000-0001-7416-038X (S.G.); 0000-0002-5154-576X (S.A.S.); 0000-0003-0606-4446 (L.L.T.); 0000-0002-5630-5714 (S.R.L.); 0000-0001-8932-0489 (R.C.); 0000-0003-1363-3985 (L.L.); 0000-0002-2020-7522 (J.R.); 0000-0003-2306-3058 (D.B.M.); 0000-0002-1446-5701 (I.V.R.).

Received for publication July 29, 2019. Accepted for publication October 9, 2019.

TCR V segments, all contribute to extreme TCR repertoire diversity, such that connections between individual MHC–peptide complexes and TCR gene segments or sequences are presently undecipherable. Discerning which of these two views is correct is not only a fundamental question for immunologists but is of potential practical importance, given rapid advances in high-throughput TCR sequencing and emerging interest in immunodiagnosis based on TCR sequence bias in peripheral blood T cells (11, 12).

Considering the entire human population, the HLA complex system uses >10,000 allomorphs to present peptides (13), but the human CD1 system uses essentially four monomorphic proteins to present Ags, and the human MR1 system uses only one. Thus, CD1 and MR1 can be thought of as genetically simple cases to test questions relating to connection of individual Ags with TCR gene bias. In the CD1 and MR1 systems, clear examples of TCR bias, which extends broadly or universally to all humans, have been identified. The most widely known example is type I NKT cells, which recognize CD1d–α-galactosylceramide complexes. In human type I NKT cells, TRAV10 genes rearrange to TRAJ18 to form identical or almost-identical TCR α-chains that pair with moderately diverse TCR β-chains. A more recently discovered example is the GEM TCR that uses TRAV1-2–TRAJ9 genes with nearly identical TCR α-chains to recognize CD1b bound to mycobacterial glucose monomycolate (GMM) Ags (14, 15). Similarly, the monomorphic MR1 displays vitamin B metabolites known as (2-oxopropylideneamino)-6-D-ribitylaminouracil (5-OP-RU) to activate human MAIT TCRs with invariant TRAV1-2–TRAJ33 α-chains (16), and coevolution between MR1 and TRAV1-2 has been suggested (17).

In these three examples, the invariant TCR α-chains pair with moderately diverse TCR β-chains to form "semi-invariant" TCRs. Within one individual and among unrelated individuals, variations of these invariant TCR α-chains are limited to a few nucleotide substitutions, which is referred to as type 3 bias (18). These three examples clearly establish linkages between named Ags and defined TCR motifs, but whether TCR bias dominates in other parts of the human CD1-reactive repertoire remains unknown. Human CD1a, CD1b, and CD1c proteins also activate T cells with diverse TCR patterns (19), and type II NKT cells that express diverse TCRs are well described for humans and mice (20–25).

Based on six clones, we previously identified a human T cell type known as LDN5-like T cells, which are named after the prototype clone, LDN5 (26). We tentatively defined LDN5-like T cells by specificity for CD1b and mycobacterial GMM, as well as the expression of TRBV4-1– or TRAV17-utilizing TCRs (27). As contrasted with type I NKT cells, MAIT cells, and GEM T cells, LDN5-like T cells show lower affinity binding to their antigenic target and much less stringent TCR sequence conservation (14, 15, 27): none of their TCR chains are invariant. In this study, we used CD1b tetramers with defined but chemically diverse lipid Ags to demonstrate a connection between CD1b recognition and TRBV4-1 expression in clones, lines, and polyclonal T cells from unrelated donors, demonstrating a broad relationship between a TCR V region and its protein target. Unexpectedly, these studies show that TRBV4-1 expression correlates with CD1b specificity but not with lipid Ag specificity. Thus, LDN5-like cells are just one example of what is actually a broader pattern of TRBV4-1 usage by CD1b-specific T cells. Finally, together with the identification of TRBV4-1 enrichment in the human CD1c-reactive T cell repertoire (28), these data spurred a crystallographic study of two CD1b-specific TRBV4-1$^+$ TCRs and mutational analysis of TCR and CD1b. These studies provide insights into how genome-encoded parts of the TRBV4-1$^+$ TCR

could potentially mediate recognition across two distinct monomorphic Ag-presenting molecules.

Materials and Methods

Protein production, Ag loading, and tetramerization

For tetramers, 20 μg of CD1b monomers obtained from the National Institutes Health tetramer facility was loaded with 32 μg of phosphatidyl-glycerol (Avanti Polar Lipids), GMM (Bill and Melinda Gates Foundation Lipid Bank), or synthetic *Borrelia burgdorferi* glycolipid II (BbGL-II; a gift from J. Kubler-Kielb, National Institutes of Health). Lipids were dissolved in citrate buffer (pH 4.5) with 0.5% CHAPS (Sigma) and incubated overnight at 37°C. After incubation, the pH was neutralized by adding Tris (pH 8.5). As negative-control CD1b monomers were treated in the same way without adding exogenous lipids. These CD1b proteins carry endogenous lipids from the expression system (CD1b-endo). CD1b mutants and wild-type (WT) control for experiments using these mutants were produced in HEK293 S GnTI$^-$ (American Type Culture Collection) and purified via HisTrap metal chelating-Ni2$^+$ affinity chromatography and size exclusion. For surface plasmon resonance (SPR), purified CD1b was loaded with a molar excess of C36 GMM (Bill and Melinda Gates Foundation Lipid Bank) over a 16-h incubation period at 20°C and purified by anion exchange chromatography. Recombinant PG10 and clone 2 TCRs were cloned into the pET30a vector, expressed in *Escherichia coli* BL21(DE3) as insoluble inclusion bodies, refolded in 20 mM Tris-HCl (pH 8.0), 5 M urea, 400 mM L-arginine, 0.5 mM Na-EDTA, 5 mM reduced glutathione, and 0.5 mM oxidized glutathione for 3 d at 273 K, and purified via size exclusion chromatography and anion exchange chromatography, until homogeneity.

Crystallization and structure determination of PG10 and clone 2 TCRs

Crystals of the PG10 and clone 2 TCRs were grown by hanging drop vapor diffusion, with a protein–mother liquor drop ratio of 1:1 at a protein concentration of 5 mg ml^{-1} in 10 mM Tris-HCl (pH 8.0) and 150 mM NaCl, with a crystallization condition of 22% (v/v) PEG 3350 and 0.2 M ammonium sulfate. Crystals were soaked in a cryoprotectant of mother liquor comprising 10% glycerol or ethylene glycol and flash-frozen in liquid nitrogen. Data were collected at the Australian Synchrotron at the MX2 Beamline (29) for both TCRs. Data were processed using the iMosflm software and scaled as part of the CCP4i Program Suite (30). Crystal structures were solved by molecular replacement using PHASER (31). Crystal structures of the PG90 TCR (Protein Data Bank accession code 5WJO; https://www.rcsb.org/structure/5WJO) and GEM42 TCR (Protein Data Bank accession code 4G8F; https://www.rcsb.org/structure/4G8F) were used as models for solving PG10 and clone 2, respectively. Manual adjustment of solved models was conducted in the Coot graphics program (32), followed by maximum-likelihood refinement using phenix.refine (31). All molecular representations were generated in PyMOL. Core root mean squared deviation (r.m.s.d.) values were calculated using Coot (32) with alignments of the TCRs that were generated against the TCR constant domains.

SPR of clone 2 and CD1b-GMM

SPR analysis of CD1b-GMM and clone 2 TCR WT and mutants was conducted on the BIAcore 3000 instrument at 20°C in 10 mM Tris-HCl (pH 8.0), 150 mM NaCl, and 0.5% (w/v) BSA. WT and mutant CD1b-GMM expressing a BirA tag were biotinylated and noncovalently coupled to a streptavidin chip. Purified refolded clone 2 in solution was passed over CD1b as the analyte at 5 μl/min. All experiments were conducted as two independent experiments in duplicate. Data analysis and visualization were conducted using GraphPad Prism 7.0, using the 1:1 Langmuir binding model.

Human subjects

PBMC were isolated from venous blood from donors in Lima, Peru, that were recruited under oversight from the Institutional Committee of Ethics in Research of the Peruvian Institutes of Health, the Institutional Review Board of the Harvard Faculty of Medicine, and the Partners Healthcare Institutional Review Board. Peruvian patients provided oral and written informed consent in Spanish and met study criteria for lack of prior tuberculosis infection, defined as negative Quantiferon test result and no clinical evidence of active tuberculosis. Separately, random blood bank donor-derived PBMC were obtained from the Brigham and Women's Hospital Specimen Bank (Boston, MA) or donated by an asymptomatic tuberculin skin test–positive subject with no clinical or radiographic

evidence of active tuberculosis at the Massachusetts General Hospital blood bank (Boston, MA).

T cell lines

The previously published primary T cell lines A25Salmonella, which contains the clones PG10 and PG90 (33), LDN5 (26), BC24A, BC24B, and BC24C (34) were grown by stimulation with 30 ng/ml anti-CD3 Ab, 25 × 10⁶ irradiated PBMC and 5 × 10⁶ irradiated EBV-transformed B cells, and 1 ng/ml IL-2, which was added on day 2 of the culture. To study tetramer binding to the GEM42 TCR, we used a TCR-transduced 5KC-78.3.20 hybridoma (14, 15). To generate primary TRBV4-1⁺ and TRBV4-1⁻ T cell lines, PBMC from random blood bank donor D43 were stained with anti-CD3 (555342; BD Biosciences) and anti–TRBV4-1 (IM2287; Beckman Coulter). Cells were sorted on a BD FACSAria (BD Biosciences), and lymphocytes were selected based on forward scatter and side scatter. A total of 1 × 10⁶ CD3⁺TRBV4-1⁺ and 1 × 10⁶ CD3⁺TRBV4-1⁻ cells were sorted. After 2 wk of stimulation as described above, both cells were stained with anti-CD3 and anti–TRBV4-1 Abs to check purity.

Single-cell TCR sequencing

To each well of a Vapor-Lock (QIAGEN)–coated 96-well plate (Eppendorf), a mixture of 0.5 μl of 5× reaction buffer, 0.5 μl of reverse transcriptase (Iscript; Bio-Rad), and 1.25 μl of H₂O was added, with a final concentration of 0.1% 4-(1,1,3,3-tetramethylbutyl)phenyl-polyethylene glycol (Triton X-100). Single cells were sorted into individual wells in this 96-well plate using a FACSAria cell sorter (BD Biosciences). The plate was centrifuged at 3000 rpm at 4°C for 10 min. For cDNA synthesis, the plate was incubated at 25°C for 5 min, followed by 42°C for 30 min and 80°C for 5 min. TCR transcripts were amplified in two subsequent nested PCRs. The primary reaction consisted of 2.5 μl of the cDNA synthesis reaction mixture as a template, 0.75 U of Taq Polymerase (Denville), 2.5 μl of 10× PCR buffer (Denville), 0.5 μl of 10 mM dNTPs, 2.5 pmol of each external TRAV and TRBV primer, 10 pmol of antisense TRAC, and 10 pmol of antisense TRBC primer as described by Wang et al. (35) in a total volume of 25 μl. The following PCR conditions were used: 95°C for 2 min; 35 cycles of 95°C for 20 s, 50°C for 20 s, and 72°C for 45 s, followed by 1 cycle of 72°C for 7 min. This reaction mixture was used as a template in two separate secondary PCRs. The mixtures are identical to the primary PCR except that in one reaction, the internal TRAV and TRAC primers were used, and in the other reaction, the internal TRBV and TRBC primers as described by Wang et al. were used (35). The following PCR conditions were used for the secondary PCR: 95°C for 2 min; 35 cycles of 95°C for 20 s, 56°C for 20 s, and 72°C for 45 s; followed by one cycle of 72°C for 7 min. PCR products were analyzed by gel electrophoresis, and α- and β-chain PCR products that resulted from the same single cell–containing well were sequenced by Sanger sequencing.

Flow cytometry

T cells (3 × 10⁶) and tetramers (0.2 μg/50 μl of staining volume) were incubated for 10 min at room temperature in PBS with 1% BSA. Subsequently, anti-CD3 (clone SK7; BD Biosciences) Ab was added and incubated for 10 min at room temperature. Subsequently, additional Abs (anti–TRBV4-1, IM2287; Beckman Coulter) were added and incubated for 20 min at 4°C. Cells were washed with PBS with 1% BSA and analyzed on an LSRFortessa (BD Biosciences) flow cytometer. For display in a matrix, percentage positive cells or mean fluorescence intensity of the positive cells was normalized to Z score, and a heat map was created using the heatmap.2 function of R (https://cran.r-project.org/web/packages/gplots/index.html).

Statistics

In Fig. 3C, significance was calculated by a paired Wilcoxon ranked sums test. Significance of the data in Fig. 1A was calculated using a Kruskal–Wallis test.

Results

TRBV4-1 TCRs recognize CD1b bound to diverse lipid Ags

A prior study of five clones (LDN5, clone 2, clone 71, clone 34, and clone 83) defined LDN5-like T cells as expressing a candidate TCR motif encoded by TRBV4-1 or TRAV17 that recognized mycobacterial GMM presented by CD1b (27). However, these clones were isolated from only four blood donors, and the distribution of LDN5-like cells among the broader human population was not determined. We designed a study in a cohort of 49 healthy donors

from Lima, Peru, that lacked positive Ag-recall tests for tuberculosis but were likely vaccinated with bacillus Calmette–Guérin according to the Peruvian national vaccination program. Besides CD1b-GMM and CD1b–mycolic acid (MA) tetramers, an Ab against TRBV4-1 was included in the cytometry panel to enable the identification of LDN5-like T cells (CD3⁺, CD1b-GMM tetramer⁺, TRBV4-1⁺). An Ab against TRAV17 might have improved identification of LDN5-like T cells, but such an Ab is unavailable. We found that TRBV4-1 usage among CD1b-GMM tetramer⁺ T cells (mean 35%) was ∼10-fold higher than among the total T cell population (3.2%; $p < 0.0001$). Thus, initial results from five clones were confirmed in a large study of polyclonal T cells among unrelated donors, demonstrating the existence LDN5-like cells as a defined, trackable T cell type in humans (Fig. 1A, Supplemental Fig. 1A).

Whereas these and prior results were generated using GMM Ag, we also observed that TRBV4-1 usage among CD1b-MA tetramer⁺ T cells (mean 26%) was also highly enriched above the total T cell population ($p < 0.0001$). This finding was unexpected because free MA lacks the glucose that has previously been demonstrated to be crucial for the recognition of GMM by LDN5 (26). This finding prompted the alignment of all available complete TCR sequences from a large panel of 26 previously published, functionally confirmed, CD1b-restricted T cell clones (19, 26, 27, 33, 34, 36–42). Similar to frequencies of TRBV4-1 expression in CD1b tetramer⁺ T cells, 11 (42%) of the CD1b-reactive clones expressed TRBV4-1 (Fig. 1B). Excluding TCRs that conform to the other known CD1b-reactive TCR motif (GEM T cells), 11 of 22 TCRs (50%) expressed TRBV4-1. These rates are well in excess of TRBV4-1 expression among randomly chosen T cells, as measured by TCR V region–specific Abs (∼1%) or by high-throughput TCR sequencing (0.5–4%) (43–45).

However, prior studies had not \tested or considered candidate TCR motifs for Ags other than the mycobacterial glycolipid GMM. Overall, this search identified at least four additional structurally distinct lipid Ags presented by CD1b to TRBV4-1–encoded TCRs: BbGL-II, sulfoglycolipid 37 (SL37), phosphatidylglycerol, and MA. Although most GMM-specific TRBV4-1⁺ clones known as LDN5-like T cells coexpress TRAV17 (27), none of the TRBV4-1⁺ clones that recognize these four other lipid Ags express TRAV17. These lipids are not structurally related to one another or to GMM with regard to lipid tails, carbohydrate groups, or inorganic sulfate or phosphate groups (Fig. 1C). In particular, the lipid head groups that protrude from the CD1b cleft (34, 46, 47) and function as TCR epitopes comprise a hexose sugar, a dihexose sugar, a phosphoglycerol unit, or a small, negatively charged headgroup with no carbohydrate, respectively (Fig. 1C). These data confirmed and extended the relationship between TRBV4-1 and CD1b reactivity but raised new questions about the specificity of TCRs for lipids carried by CD1b. In particular, could TRBV4-1 sequences mediate recognition of CD1b while ignoring the Ag carried by CD1b, while other parts of the TCR are available for Ag recognition?

CD1b-specific T cells among polyclonal T cell lines

Because these T cell clones were derived with diverse methods and from genetically unrelated donors, we carried out controlled experiments in which TRBV4-1⁺ and TRBV4-1⁻ cells were sorted from the PBMC of the same blood bank donor, D43, and cultivated in parallel under equivalent conditions. Using an mAb that binds to TCRs that use TRBV4-1, equal numbers of CD3⁺TRBV4-1⁺ and CD3⁺TRBV4-1⁻ T cells were sorted (Supplemental Fig. 1B) and expanded by stimulation with anti-CD3 Ab, after which the uniform expression or absence of
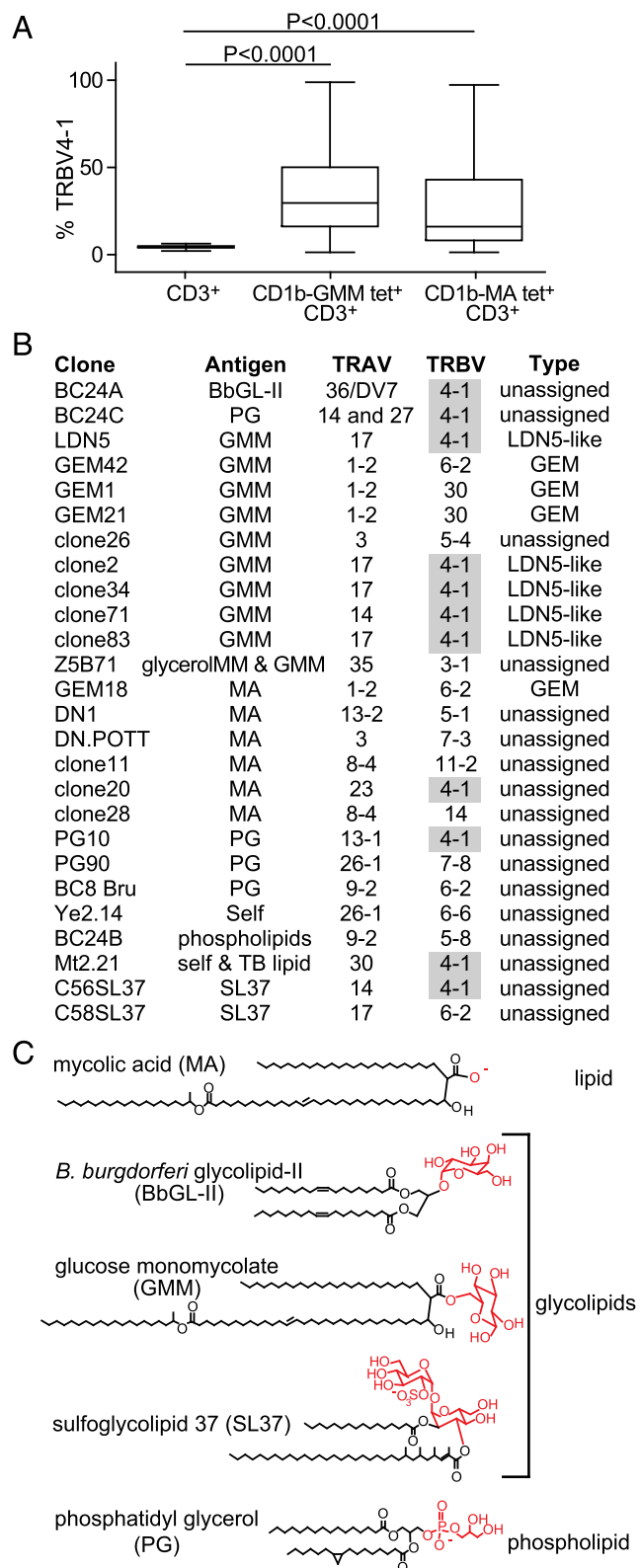
A

B

Clone	Antigen	TRAV	TRBV	Type
BC24A	BbGL-II	36/DV7	4-1	unassigned
BC24C	PG	14 and 27	4-1	unassigned
LDN5	GMM	17	4-1	LDN5-like
GEM42	GMM	1-2	6-2	GEM
GEM1	GMM	1-2	30	GEM
GEM21	GMM	1-2	30	GEM
clone26	GMM	3	5-4	unassigned
clone2	GMM	17	4-1	LDN5-like
clone34	GMM	17	4-1	LDN5-like
clone71	GMM	14	4-1	LDN5-like
clone83	GMM	17	4-1	LDN5-like
Z5B71	glycerolMM & GMM	35	3-1	unassigned
GEM18	MA	1-2	6-2	GEM
DN1	MA	13-2	5-1	unassigned
DN.POTT	MA	3	7-3	unassigned
clone11	MA	8-4	11-2	unassigned
clone20	MA	23	4-1	unassigned
clone28	MA	8-4	14	unassigned
PG10	PG	13-1	4-1	unassigned
PG90	PG	26-1	7-8	unassigned
BC8 Bru	PG	9-2	6-2	unassigned
Ye2.14	Self	26-1	6-6	unassigned
BC24B	phospholipids	9-2	5-8	unassigned
Mt2.21	self & TB lipid	30	4-1	unassigned
C56SL37	SL37	14	4-1	unassigned
C58SL37	SL37	17	6-2	unassigned

C

FIGURE 1. TRBV4-1$^+$ CD1b-restricted clones recognize a wide variety of Ags. (**A**) PBMC from 49 healthy donors were pregated for CD3 expression and CD1b-GMM tetramer or CD1b-MA tetramer binding (Supplemental Fig. 1A). Within the tetramer$^-$ or tetramer$^+$ gates, the percentage of TRBV4-1–expressing cells was determined. Box: median with interquartile range; whiskers: minimum to maximum values. (**B**) Previously published CD1b-restricted TCRs are shown according to V (TRAV, TRBV) genes and the Ag they recognize: LDN5 (26); GEM1, GEM18, GEM21, and GEM42 (27); clone 2, clone 26, clone 34, clone 71, clone 83 (27); Z5B71 (36); DN1 (37); DN.POTT (19, 38); PG10, PG90,

TRBV4-1 by the cell lines was confirmed (Fig. 2A). Both T cell lines were stained with CD1b tetramers that were mock-treated, and so contained diverse cell-derived endogenous lipids (CD1b-endo), or were loaded with phosphatidylglycerol or GMM as examples of structurally divergent phospholipid or glycolipid Ags. In the TRBV4-1$^+$ polyclonal T cell line, there was an increased frequency of cells that bind to CD1b-phosphatidylglycerol or CD1b-GMM compared with the TRBV4-1$^-$ population (Fig. 2B). Thus, TRBV4-1$^+$ is more likely to confer CD1b reactivity than the combined action of the other Vβ segments. Furthermore, the CD1b reactivity is not limited to CD1b bound to one specific Ag. In fact, phosphatidylglycerol and GMM are very different, as structural studies of TCR–CD1b–lipid complexes show that they use distinct glucose versus phosphoglycerol units on the TCR-facing surface of CD1b (14, 46).

Confirming TRBV4-1 expression, single-cell TCR sequencing demonstrated that among the CD1b-phosphatidylglycerol binding cells were several single cells that expressed identical pairs of α- and β-chains composed of TRAV8-2–TRAJ38 and TRBV4-1–TRBJ1-6. Likewise, among cells that bind to CD1b-GMM were several cells that expressed identical pairs of α- and β-chains composed of TRAV13-2–TRAJ32 and TRBV4-1–TRBJ1-4 (Fig. 2C). Even though in healthy blood bank–derived donors, the frequency of GMM- and phosphatidylglycerol-specific cells is typically below or at the detection limit of $\sim 10^{-4}$, pre-enrichment for TRBV4-1 apparently enriches for CD1b-specific cells to a level that they can now be detected.

CD1b-specific T cells among TRBV4-1$^+$ T cells ex vivo

To bypass artifacts related to T cell culture and outgrowth, we next analyzed polyclonal T cells directly ex vivo. We used fresh PBMC from three random blood bank donors (D6, D7, and D48) and costained them with anti-CD3, anti–TRBV4-1, and CD1b tetramers treated with the phospholipid phosphatidylglycerol or the glycolipid GMM to measure the rate of staining with tetramers in the TRBV4-1$^+$ T cell gate (Fig. 2D, 2E). As negative controls, we measured staining with mock-treated CD1a tetramers (Supplemental Fig. 1C) and CD1b tetramer staining in the TRBV4-1$^-$ gate (Fig. 2D, 2E). In all three donors, we detected a higher percentage of cells that stain with CD1b-phosphatidylglycerol or CD1b-GMM tetramers in the TRBV4-1$^+$ population compared with the TRBV4-1$^-$ population (Fig. 2E) or any T cell population stained with CD1a tetramers (Supplemental Fig. 1C). Most tetramer$^+$ T cells stained with both tetramers, which suggests that they represent a broadly cross-reactive population that has been described previously (34). The lack of T cells that were single-positive for the CD1b-GMM tetramer is most likely due to extremely low frequencies of CD1b-GMM$^+$ T cells among blood bank donors in Boston, who are most likely not exposed to bacillus Calmette–Guérin vaccine or *Mycobacterium tuberculosis*. Overall, enrichment of CD1b tetramer$^+$ cells among TRBV4-1$^+$ T cells was confirmed directly ex vivo. Thus, polyclonal T cells from genetically unrelated donors provided a new and strong linkage between TRBV4-1 TCR expression and CD1b recognition.

and BC8 Bru (33); YE2.14 (39); MT2.21 (40); C56SL37 and C58SL37 (41); and clone 11, clone 20, clone 28 (42), BC24A, BC24B, and BC24C (34). BC24C expresses two different α-chains. (**C**) Lipid Ags illustrate the structural diversity of molecules, with polar head groups indicated in red, recognized by TRBV4-1 TCRs.
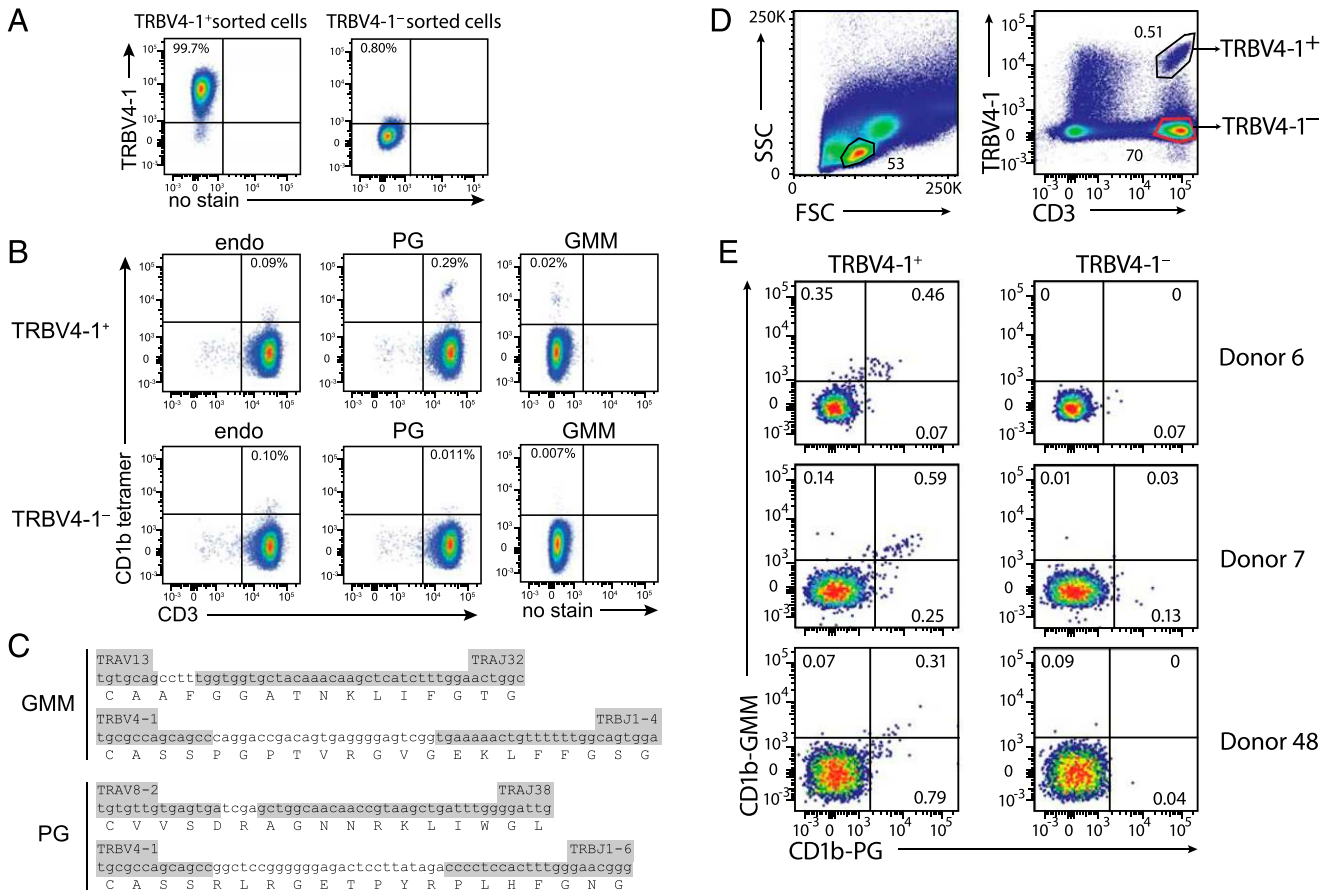
FIGURE 2. CD1b recognition by TRBV4-1^{+} T cells. (**A**) Cell lines sorted from blood bank donor D43 based on expression or absence of TRBV4-1 (Supplemental Fig. 1B) were tested for TRBV4-1 expression. (**B**) Both cell lines were stained with CD1b-phosphatidylglycerol (PG) or CD1b-GMM tetramers or mock-loaded CD1b tetramers carrying diverse endogenous lipids (CD1b-endo). (**C**) TCR sequences obtained by single-cell TCR sequencing of CD1b-GMM tetramer[+] and CD1b-phosphatidylglycerol (PG) tetramer^{+} cells are shown with germline (gray) and nongermline (white) residues encoded by the indicated V and J region genes. After pregating using anti-CD3 and anti–TRBV4-1 TCR Abs (**D**), TRBV4-1[+] and TRBV4-1^{−} T cells from PBMC from three random blood bank donors were analyzed for binding of CD1b-phosphatidylglycerol (CD1b-PG) and CD1b-GMM tetramers directly ex vivo (**E**). Equal numbers of cells are shown in each plot. All acquired TRBV4-1^{−} cells are shown in Supplemental Fig. 1B (top).

High-throughput sequencing of TCR rearrangements in CD1b tetramer[+] and tetramer^{−} T cells

Next, we used high-throughput TCR sequencing (Adaptive Bio-technologies, Seattle, WA) to measure the TRBV gene usage in functional TCR rearrangements among T cells that were sorted into CD1b tetramer[+]–enriched and CD1b tetramer[−] populations (Fig. 3). We chose MA as the ligand for CD1b tetramers based on its antigenic properties in the CD1 system (19, 37, 42), including its stimulation of polyclonal (Fig. 1A) and clonal (Fig. 1B) TRBV4-1^{+} T cells. In Boston, MA, we obtained PBMC from two blood bank donors (CX and C63) and one person who was latently infected with *M. tuberculosis* (C58). T cells were stimulated once with autologous monocyte-derived dendritic cells and MA and cultured for 17 d prior to sorting into CD1b-MA tetramer[+] and CD1b-MA tetramer[−] populations (Supplemental Fig. 1D). The junctional regions of their TCRs were sequenced in high throughput and their V genes assigned, showing that tetramer^{+} cells used TRBV4-1 at markedly increased rates for donors CX and C58 (Fig. 3A, green arrows). In donor C63, the postsort analysis demonstrated high contamination with tetramer^{−} cells (92.6%) in the tetramer^{+} cells (Supplemental Fig. 1D), so a sort failure explained the highly similar profiles for TRBV genes in this patient.

To increase the number of known Ags and donors analyzed, we took advantage of a publicly available dataset that used a similar approach based on CD1b-GMM tetramer sorting for high-throughput TCR sequencing (48). Similar to CD1b-MA tetramer results, all four patients analyzed with CD1b-GMM tetramers showed marked enrichment of TRBV4-1 among tetramer[+]-enriched cells as compared with tetramer^{−} cells (Fig. 3B). Overall, TRBV4-1 use among CD1b tetramer[+]–enriched polyclonal T cells was higher in all six subjects studied, and the result was statistically significant ($p = 0.016$) (Fig. 3C). Furthermore, because MA and GMM are chemically distinct Ags and TCRs specific for one do not typically cross-react with the other (14, 15, 26, 27, 49), preferred expansion of TRBV4-1^{+} cells by both Ags suggests that TRBV4-1 is driving CD1b recognition rather than lipid Ag recognition, in agreement with the clonal T cell analyses (Fig. 1).

Detectable TCR conservation is limited to the V gene

TRBV4-1 encodes all CDR1β and CDR2β amino acids and the first 4 aa of CDR3β. The C-terminal part of CDR3β is encoded by non–germline-encoded N nucleotides, D segments, and part of the J segment. To develop hypotheses about which TCR β-chain residues could interact with CD1b, we examined the known CD1b-reactive, TRBV4-1[+] β-chain sequences in more detail. Among 12 TRBV4-1[+] TCRs that recognize CD1b in combination with differing lipid, glycolipid, or phospholipid Ags, we observed no enrichment for any single TRBJ segment or a preference for TRBJ segments that belong to the TRBC1 or TRBC2 groups (Fig. 4A). Furthermore, we could not discern CDR3β common
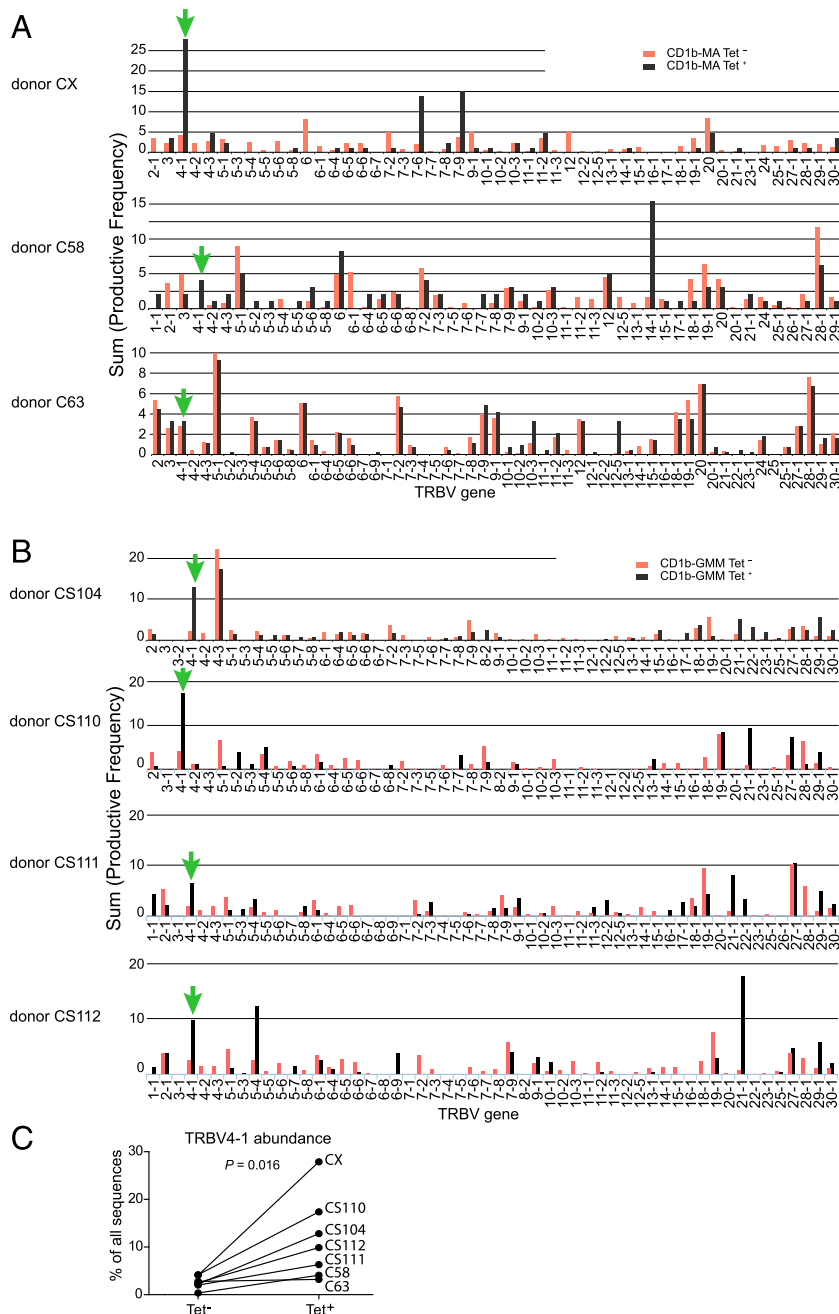
FIGURE 3. TRBV4-1^{+} T cells are enriched among CD1b tetramer^{+} T cells. (**A**) PBMC from three blood donors were stimulated with autologous monocyte-derived dendritic cells and MA for 18 d. The resulting cells were stained with CD1b-MA tetramers and an anti-CD3, followed by sorting of tetramer[+] and tetramer^{−} cells as shown in Supplemental Fig. 1D, and subjected to high-throughput TCR sequencing. The percentages of TRBV gene usage are shown. (**B**) Using the approach described above, we reanalyzed a publicly available dataset (48) of CD1b-GMM tetramer[+] and tetramer^{−} cells from four donors. (**C**) Summary of TRBV4-1 percentages among tetramer[+] and tetramer^{−} cells of the three donors shown in (A) and four donors shown in (B).

sequence patterns beyond the TRBV4-1–encoded residues at positions 104–107 (CASS). This is in sharp contrast with MAIT, NKT, and GEM TCRs, which have TCR α-chains that are nearly identical in length and sequence, including CDR3α regions, and are formed by identical V and J segments. Therefore, further studies investigated the hypothesis that TRBV4-1–encoded residues might mediate recognition of CD1b.

Structural analysis of conserved TRBV4-1 TCRs

First, we focused on the residues encoded by TRBV4-1 that encode CDR1β (MGHRA), CDR2β (YSYEKL), and the first four residues of CDR3β (CASS) (Fig. 4A). For a detailed understanding of where these residues are positioned within αβ TCR heterodimers, we cloned two TRBV4-1[+] CD1b-reactive TCRs (clone 2 and PG10 TCRs), expressed them as heterodimeric proteins, and determined their structures to 1.8 and 2.5 Å resolution, respectively (Fig. 4B, Supplemental Table I). The clone 2 TCR recognizes CD1b-GMM (27) and so represents an LDN5-like TCR. The

PG10 TCR recognizes CD1b-phosphatidylglycerol and so represents the non–GMM-specific TRBV4-1[+] TCR motif identified in this study (33). These were compared with two existing structures of TRBV4-1[−] TCRs: a GEM TCR (GEM42) and a phosphatidylglycerol-CD1b-reactive TCR (Fig. 4B).

Structural comparisons between the TRBV4-1[+] and TRBV4-1[−] TCRs reveals extensive electropositive regions at the Ag-recognition site. Compared with PG90 and GEM42 TCRs, the TRBV4-1[+] TCRs exhibit greater electropositivity in a region located predominantly between the CDR3 loops, extending toward the CDR2β loop (Fig. 4B, blue). This electropositive feature correlates with the electronegative surface of the CD1b Ag-binding cleft (Fig. 4C, red). As previously determined cocrystal structures of PG90-CD1b-phosphatidylglycerol and GEM42-CD1b-GMM demonstrate selective corecognition between an electropositive TCR interface and electronegative CD1b (14, 34), a broadly similar mode of docking for the TRBV4-1[+] TCRs onto CD1b might potentially operate.
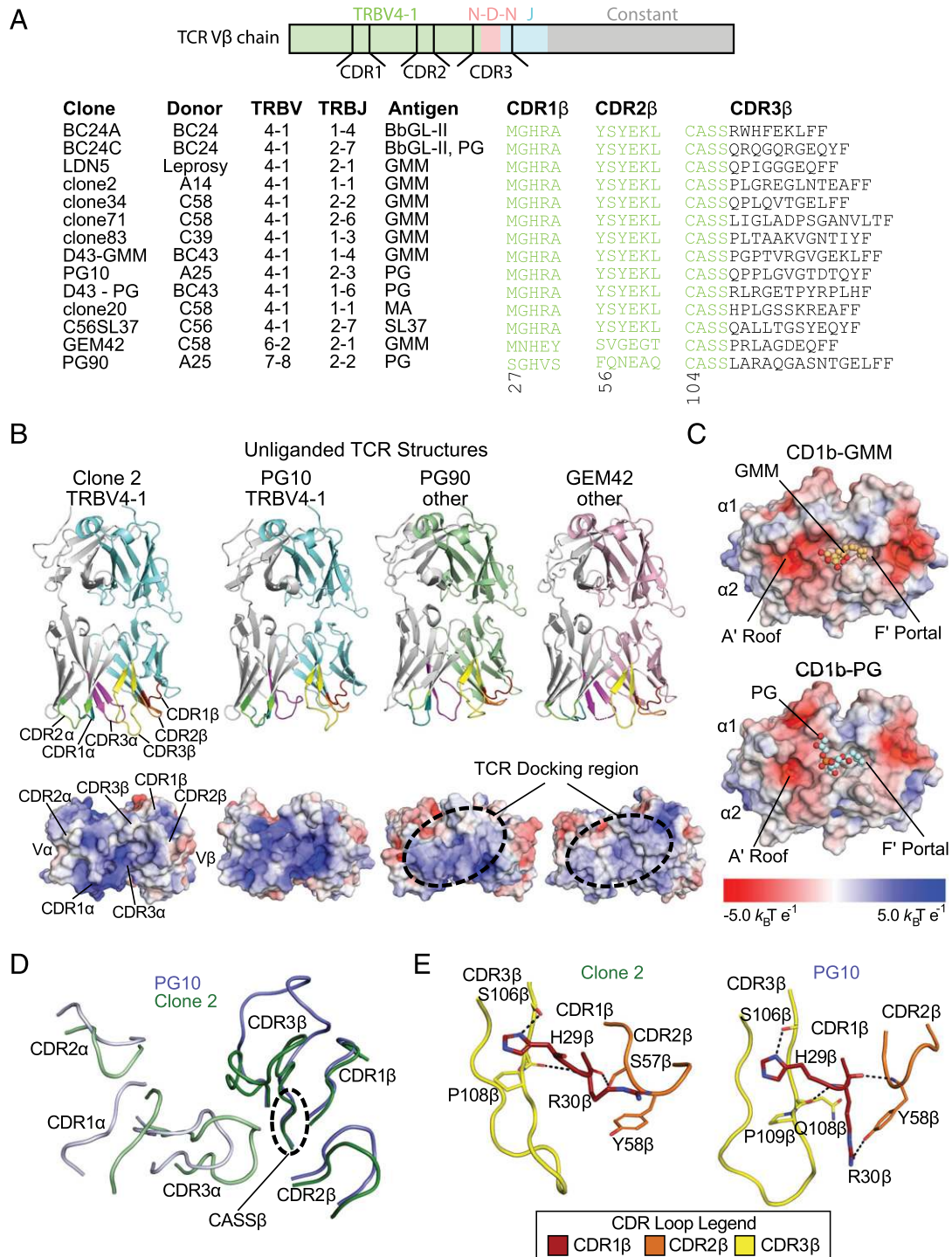
FIGURE 4. Structural analysis of TRBV4-1[+] TCRs. CD1b-specific TRBV4-1[+] TCR conservation is limited to the germline-encoded TRBV gene. (**A**) The schematic shows the role of TRB locus genes in encoding residues in the CDR1, CDR2, and CDR3 regions. CDRβ regions of new and previously sequenced TRBV4-1[+] and TRBV4-1[−] CD1b-specific clones were aligned. BbGL-II is 1,2-di-oleyl-a-galactopyranosyl-sn-glycerol; SL37 is synthetic di-acylated sulfoglycolipid analog (67). (**B**) Upper, Side view of clone 2, PG10, PG90, and GEM42 TCRs, with α-chains (gray), TRBV4-1 β-chains (cyan), and other β-chains (green and pink) highlighted. Lower, Bottom-up view of TCR interface surface electrostatic potential. (**C**) In comparison, top-down view of the CD1b interface surface electrostatic potential is shown, with CD1b presenting GMM (brown, upper) and phosphatidylglycerol (PG) (blue, lower). Potential contours are shown on a scale from +5.0 (positive charge, blue) to −5.0 $k_B T\,e^{-1}$ (negative charge, red); white indicates value close to 0 $k_B T\,e^{-1}$ (neutral charge). (**D**) Overlay image shows CDR regions of clone 2 (green) and PG10 (blue) TCRs. (**E**) Key interactions in the TRBV4-1[+] CDRβ regions are shown, including positions of H29β and R30β on the CDR2β region of clone 2 (green, left) and PG10 (blue, right) TCRs. Amino acid residues involved in contacts are represented as sticks, with hydrogen bonds represented as black dashes. Nitrogen, oxygen, and phosphate are represented in blue, red, and orange, respectively, and color coding of CDR regions is highlighted in the legend.

Despite the different lipid Ags recognized, the overall positioning of the Cα carbon backbone, the amino acid residue side chain position in the CDR1β loop, and the germline-encoded

CASS region of the CDR3β loop were highly conserved between the two TRBV4-1[+] TCRs, with r.m.s.d. values of 0.2 and 0.1 Å, respectively (Fig. 4D). The CDR2β loop of the clone 2

TCR is involved in crystal contacts and, as such, aligned less well to the PG10 TCR CDR2β loop (r.m.s.d. value of 1.3 Å). Notably, the position of H29β in the CDR1β loop is highly conserved in both TCRs, being wedged between the germline-encoded S106β and P108β residues of the CDR3β region (Fig. 4E). H29β appears to play a stabilizing role that anchors the germline-encoded N-terminal end of the CDR3β loop via hydrogen bond formation with S106β. In turn, the main chain carbonyl group of H29β is stabilized via hydrogen bonds by the CDR2β residues S57β or Y58β (Fig. 4E). Of interest, a similar interaction is observed in the two non–TRBV4-1 TCRs, PG90 and GEM42. Despite using TRBV7-8 and TRBV6-2, respectively, H29β is also encoded in the CDR1β region (Fig. 4A) and stabilizes the germline-encoded CDR3β region. By analogy to the known docking modes of PG90 and GEM42 TCRs (Supplemental Fig. 2), this inter–CDR1β–CDR3β region is positioned distally to the CD1b–lipid–TCR interface, where it acts to stabilize the CDR3β region to allow for direct lipid headgroup contact. In the absence of a trimolecular TRBV4-1$^+$ TCR–CD1b–lipid structure, it is unclear whether H29β plays a similar role when the TCR uses TRBV4-1.

Although H29β is conserved in these four TCRs, R30β is present only in the two TRBV4-1$^+$ TCRs (Fig. 4A). In this study, R30β was solvent-exposed and adopted two distinct conformations in the clone 2 and PG10 TCRs (Fig. 4D). In the PG10 TCR structure, R30β hydrogen bonds with Y58β, where the residue contributes toward the electropositive interface surface of the PG10 TCR. In the clone 2 TCR structure, R30β is orientated away from the interface in a manner not related to crystal contacts (Fig. 4D), and as such, the interface surface is less electropositive (Fig. 4B). Because of the electrostatic complementary nature of the TCR and CD1b interface and the positioning of R30β toward the interface surface in the PG10 TCR structure, this residue might be involved in contacts between CD1b and TRBV4-1.

Mapping of essential residues in the CD1b–clone 2 TCR interaction

These crystal structures guided additional alanine substitution experiments to test which TRBV4-1 CDR residues are crucial for recognition of CD1b-GMM by the clone 2 TCR. Mutations along the CDR1β and CDR2β regions were generated, but recombinant protein production was reduced dramatically with CDR2β mutants. The side chains of these residues are solvent-exposed, so changes of this type are known to affect overall protein solubility and integrity. To bypass this technical limitation, we mutated CDR1β amino acid H29β, R30β, and a framework region 1 residue, T16, as a negative control. SPR experiments were performed to measure steady-state binding affinities between these TCR mutants and GMM-loaded CD1b monomers coupled to a sensor chip. The K_D of WT clone 2 TCR and the T16A mutant were comparable: 6.9 ± 1.0 and 6.1 ± 0.6 μM, respectively (Fig. 5A). However, both mutations in the CDR1β region showed a marked decrease in CD1b-GMM binding affinity, resulting in a K_D of >200 μM (Fig. 5A). This indicates that the H29β and R30β are critical TRBV4-1$^+$ residues for mediating high-affinity TCR interactions with CD1b-GMM. Based on the locations of the residues in the CDR1 loop, such effects are likely mediated via an indirect (H29β) or direct (R30β) impact on TRBV4-1 docking onto CD1b.

Next, we carried out alanine scanning mutation across the surface of CD1b to functionally evaluate the CD1b–clone 2 TCR interaction via SPR (Fig. 5B). As the goal was to specifically assess the TCR–CD1b interaction interface, we did not mutate sites that function as interdomain tethers to control Ag entry into

the cleft (D60, E62) (50). Instead, we studied 10 alanine point mutants on the outer surface of CD1b, which are located on the TCR-facing aspect of the α1 (E65A, I69A, V72A, R79A, E80A) and α2 (Y151A, I154A, T157A, R159A, I160A) helices, as determined from prior crystal structures (14, 51). Only E80A (nonbinding), Y151A (nonbinding), I154A (nonbinding), and T157A (38.9 ± 8.3) mutants demonstrated a significant reduction in steady-state affinities, resulting in significantly reduced or abrogated clone 2 TCR binding onto CD1b-GMM (Fig. 5B).

Consistent with this interpretation, most human CD1 group 1–reactive TCRs, including all three of the known CD1b-binding αβ TCRs (14, 34, 46), bind CD1 such that the TCR α-chain is positioned over the A′-roof, distant from the hot spot established there. The established hot spot that significantly affects clone 2 TCR binding resides at the F′ portal and involves E80 and Y151 (Fig. 5C). As observed with the GEM42 and PG90 TCRs, this site is critical for TCR β-chain interaction with CD1b (14, 46).

Conserved functional hot spots for all TRBV4-1$^+$ TCRs

Next, we wanted to determine if any CD1b residues are important in the interaction with the broader spectrum of CD1b-reactive TCRs. First, we assembled a panel of TRBV4-1$^+$ (LDN5, PG10, D43, BC24C) and TRBV4-1$^-$ Ag-specific, CD1b-reactive clones (BC24B, PG90, GEM42). These clones were evaluated for staining with human CD1b tetramers that were treated with the relevant glycolipid (GMM) or phospholipid (phosphatidylglycerol) Ag and CD1a tetramers as a negative control. At the same time, 13 alanine-substituted CD1b proteins (K61A, E65A, E68A, I69A, V72A, R79A, E80A, Q150A, Y151A, Q152A, E156A, I160A, and E164A) were assembled into tetramers, mock- or Ag-treated, and then tested on all clones to map the functional interaction sites on CD1b. Finally, the clone BC24B was known to show autoreactive response to mock-loaded CD1b and phosphatidylglycerol-treated CD1b, so it was tested with all mutant tetramers prepared in mock and phosphatidylglycerol loading conditions. This tetramer-based biophysical approach was chosen because it emphasized clonal TCR binding to defined combinations of CD1b and lipid Ag. The use of staining instead of cytokine release eliminated clone-to-clone differences in activation outcomes downstream of TCR ligation. Furthermore, as compared with cellular assays, this approach minimized the effects of APC-derived lipid Ags or differential processing of phosphatidylglycerol or GMM Ags. Analysis of staining of LDN5 and GEM42 by CD1b-GMM tetramers (Fig. 6A) and PG10 and BC24B by CD1b-phosphatidylglycerol tetramers (Fig. 6B) illustrates key outcomes, which, when combined with results from the additional four staining patterns (Supplemental Fig. 3A–D), generated a matrix of staining results (Fig. 6C).

No tetramer stained every T cell clone, and in no case did CD1a tetramers stain T cells. These two findings largely rule out nonspecific interaction of tetramers with lymphocytes. Every CD1b tetramer–Ag combination stained at least one T cell line, demonstrating that no mutant tetramer failed to fold or load lipid. In all cases, dependence on the glycolipid or phospholipid matched the known Ag specificity of the clone, consistent with the interactions being mediated by TCRs interacting with combinations of CD1b and Ag. As measured by the percentage of cells staining above background (Fig. 6C) or mean fluorescence intensity (Supplemental Fig. 3E), the matrix staining conditions demonstrated clear, CD1b position-dependent changes in staining and linked these to the Ag and TCR type used.

Except for the K61A mutation, which had little effect compared with WT CD1b, most mutations had a different effect on tetramer binding, depending on which T cell line was tested. Thus, TCR
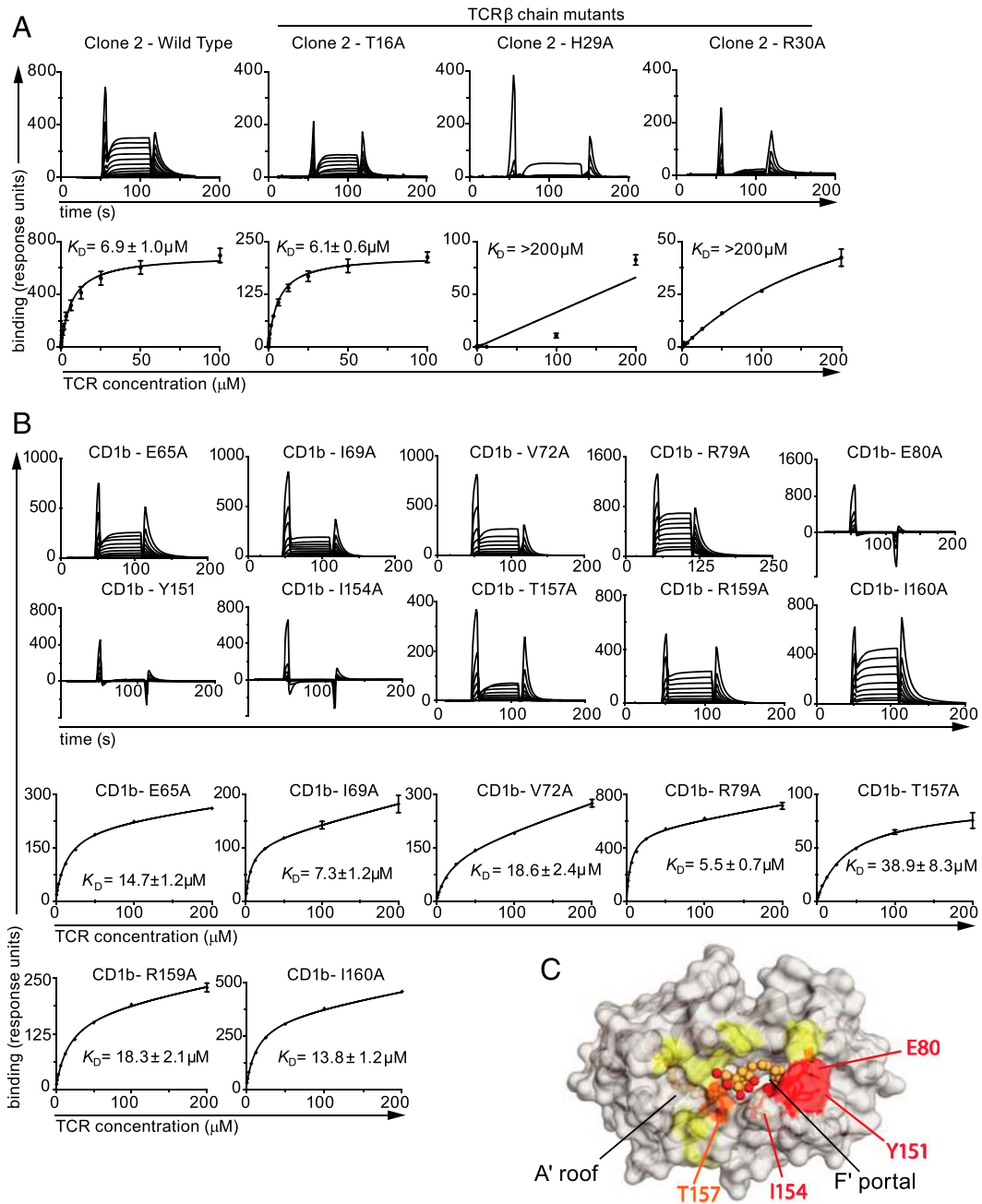
FIGURE 5. Mutational analysis of the TCR–CD1b interaction. (**A**) CD1b-reactive clone 2 TCR was expressed as a heterodimer encoded by WT sequences or subjected to β-chain point mutation with alanine substitutions in the TRBV4-1–encoded region at position 29 or 30. Binding to GMM-loaded CD1b complexes was measured using SPR to generate steady-state affinities, with binding curves (upper) and equilibrium curves (lower) shown. (**B**) The steady-state affinities of the WT clone 2 TCR for WT and mutant CD1b proteins loaded with GMM were determined. Equilibrium curves for CD1b-E80A, CD1b-Y151A, and CD1b-Y154A showed no observable binding. Error bars represent mean ± SEM. (**C**) Surface representation of the CD1b-GMM surface (white) with residues when mutated to alanine demonstrate less than a 3-fold decrease in affinity (yellow), a 3–5-fold decrease in affinity (orange), and greater than a 5-fold decrease (red), upon binding against the clone 2 TCR. Positions of residues E80, Y151, I154, and T157 are indicated.

interactions with CD1b were not precisely conserved, especially for the diverse TRBV4-1⁻ TCRs (Fig. 6C). However, there was a striking commonality among all four TRBV4-1⁺ T cells tested: mutation of the E80A on CD1b abolished recognition. This outcome was true regardless of whether GMM or phosphatidylglycerol was carried. The E80A CD1b tetramers were not nonfunctional in a general way, based on positive results with other clones, and both phosphatidylglycerol and GMM were loaded, as assessed by bright staining BC24B and GEM42 (Fig. 6A, 6C). These patterns demonstrate that E80 in CD1b is an important residue for

interaction with TRBV4-1–encoded TCRs, establishing a functional hot spot for TRBV4-1⁺ TCRs that acts independently of the Ag loaded.

Discussion

T cells recognizing monomorphic Ag-presenting molecules represent an important exception to the general idea that specific TCR sequences cannot be linked to the molecular identity of the antigenic targets recognized. Through study of polyclonal T cells from genetically unrelated donors, our new data show that CD1b
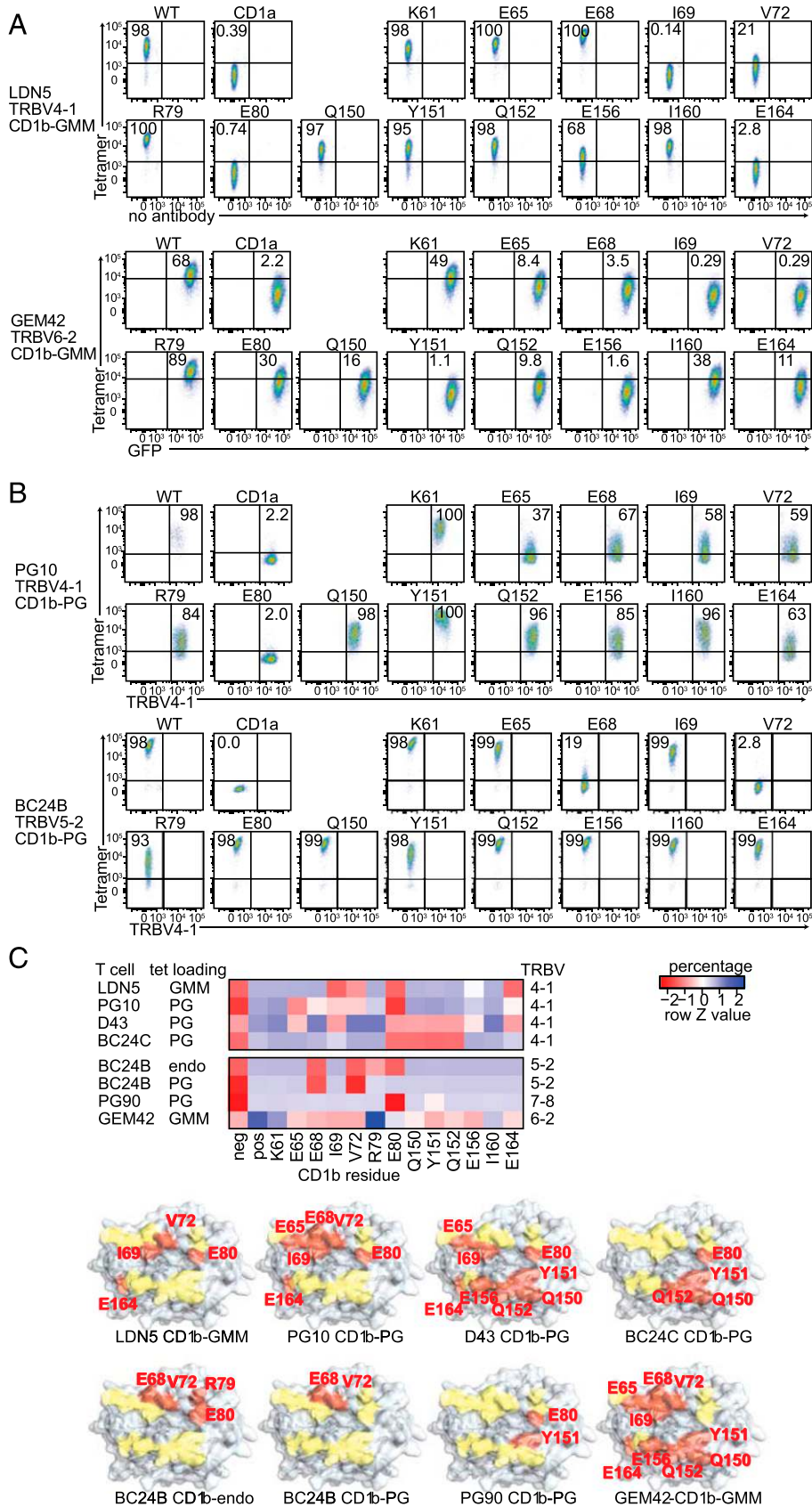
FIGURE 6. The effect of mutations in CD1b on interaction with T cells. (**A**) T cell clones LDN5 and GEM42 were tested for binding of GMM-loaded CD1b tetramers with the indicated point mutations. (**B**) T cell clones PG10 and BC24B were tested for binding of phosphatidylglycerol-loaded CD1b tetramers (CD1b-PG) with the indicated point mutations. (**C**) In addition, four additional T cell clone–CD1b–Ag combinations were tested (Supplemental Fig. 3A–D), and percentages of tetramer^{+} cells or mean fluorescence intensity (Supplemental Fig. 3E) were Z score–normalized per cell line and shown as a heat map. The negative control (neg) is mock-loaded WT CD1a tetramer, and the positive control (pos) is the indicated Ag-loaded WT tetramer.

tetramer^{+} cells are enriched among TRBV4-1^{+} cells in vitro and ex vivo. Conversely, among CD1b-specific clones and polyclonal CD1b tetramer^{+} T cells, TCR sequencing demonstrated markedly increased use of TRBV4-1. Thus, bidirectional evidence supports linkage between TRBV4-1 expression and CD1b recognition. CD1b-restricted T cells expressing TRBV4-1[+] TCRs represent a population of which LDN5-like T cells form a subset that is defined by recognition of GMM.

MAIT cells, type I NKT cells, and GEM T cells express TCRs with invariant α-chains and mediate highly specific responses to 5-OP-RU, α-GalCer, and GMM, respectively. CD1b-specific T cells described in this study differ from the known TCR-defined T cell types in several ways. First, TCR sequence motifs are found in the TCR β-chains, not the TCR α-chains. Second, the TCRs show a lower degree (type 1 bias) of conservation that is restricted to the TRBV4-1 gene segment, rather than multiple segments or N region additions. Third, and most surprisingly, even though each individual TRBV4-1[+] TCR that we studied in this study is specific for a lipid Ag, the TRBV4-1 motif biases toward CD1b recognition without regard to the Ag carried. A recent study independently established a link between TRBV4-1 and CD1c recognition (28). The broad Ag response pattern for TRBV4-1^{+} T cells is, to our knowledge, unprecedented, in the sense that one germline-encoded part of a TCR acts without regard to the Ag carried and likely reacts across two types of Ag-presenting molecules. For MAIT cells, NKT cells, and GEM T cells, the recognition mechanism is straightforward and well-proven: the particular residues encoded by TRAV and TRAJ regions of each of these invariant TCR α-chains make extensive physical contact with MR1, CD1d, or CD1b and protruding epitopes on the carried lipid or metabolite Ags (14, 52–54). Our data show that the shared TCR features are found in the germline residues of TRBV4-1 but not in N region or TRBJ residues that dominate the CDR3 loop. Therefore, a straightforward structural explanation for these functional responses would be that residues encoded by TRBV4-1 recognize some shared epitope on CD1b and CD1c that does not involve the carried lipid.

Although direct proof of the molecular mechanism requires ternary TRBV4-1 TCR–CD1b crystal structures, much existing evidence points toward specific roles of TRBV4-1 sequences in TCR stabilization and binding to anionic surfaces on CD1b and CD1c. First, TCR crystal structures of clone 2 and PG10, as well as mutational scanning, pinpointed roles of two TRBV4-1–encoded residues, H29β and R30β. H29, which forms a hydrogen bond between the CDR1 and CDR3 loops, is located distally from the TCR surface, and so not expected to directly contact CD1b or Ag, but could stabilize the general internal structure of TCRβ. However, this intrachain, interloop interaction is common among non–TRBV4-1 TCRs and so does not likely account for their CD1-biasing nature. Instead, the positively charged residue R30β, which is found only in TRBV4-1, TRBV5-1, and TRBV10-3, is well-positioned to contact CD1b. Also, published mutational mapping independently implicates R30 of TRBV5-1 as crucial for TCR interaction with CD1b (55), and R30β of TRBV4-1 is crucial for the interaction with CD1c (28).

On the CD1 side, our mutational mapping for CD1b implicated E80, an anionic residue, as essential for binding of all five TRBV4-1[+] TCRs tested in this study. E80 is necessary for a TRBV5-1[+] and one other TRBV4-1[+] CD1b-specific TCR response (40). E80 is also found in CD1c but not in CD1a and CD1d, so its presence correlates with the two isoforms recognized by TRBV4-1 TCRs (56). Although no TRBV4-1 TCR has been solved in contact with CD1b, most αβ TCR–lipid–CD1 structures, and all three ternary CD1b structures solved to date, show that CDR1β and CDR2β loops that carry R30 are positioned near the right margin of the CD1 platform, where E80 is also located (14, 34, 46). Overall, these data support a potential scenario in which the conserved, positively charged residue R30 could bind CD1b near the negatively charged E80, although other anionic residues are present on the CD1b surface. Finally, *CD1B* and *CD1C* genes encoding E80 are widely present among mammals (57–63). No *CD1B* or *CD1C* (64) orthologs are present in mice, and mice lack a *TRBV4-1*

ortholog (65, 66). Therefore, analogous to the simultaneous presence or absence of *MR1* and *TRAV1-2* orthologs among mammals (17), a comparable coevolutionary relationship might exist between *TRBV4-1* and *CD1B* or *CD1C* orthologs. These data, and the availability of human tetramers made from nonpolymorphic Ag-presenting molecules, now provide new avenues to discovering hidden TCR patterns in the complex human TCR repertoire.

Disclosures

The authors have no financial conflicts of interest.

References

1. Salio, M., J. D. Silk, E. Y. Jones, and V. Cerundolo. 2014. Biology of CD1- and MR1-restricted T cells. *Annu. Rev. Immunol.* 32: 323–366.
2. Han, M., L. I. Hannick, M. DiBrino, and M. A. Robinson. 1999. Polymorphism of human CD1 genes. *Tissue Antigens* 54: 122–127.
3. Van Rhijn, I., and D. B. Moody. 2015. Donor unrestricted T cells: a shared human T cell response. *J. Immunol.* 195: 1927–1932.
4. Rossjohn, J., S. Gras, J. J. Miles, S. J. Turner, D. I. Godfrey, and J. McCluskey. 2015. T cell antigen receptor recognition of antigen-presenting molecules. *Annu. Rev. Immunol.* 33: 169–200.
5. Garcia, K. C., M. Degano, R. L. Stanfield, A. Brunmark, M. R. Jackson, P. A. Peterson, L. Teyton, and I. A. Wilson. 1996. An alphabeta T cell receptor structure at 2.5 A and its orientation in the TCR-MHC complex. *Science* 274: 209–219.
6. Garboczi, D. N., U. Utz, P. Ghosh, A. Seth, J. Kim, E. A. VanTienhoven, W. E. Biddison, and D. C. Wiley. 1996. Assembly, specific binding, and crystallization of a human TCR-alphabeta with an antigenic Tax peptide from human T lymphotropic virus type 1 and the class I MHC molecule HLA-A2. *J. Immunol.* 157: 5403–5410.
7. La Gruta, N. L., S. Gras, S. R. Daley, P. G. Thomas, and J. Rossjohn. 2018. Understanding the drivers of MHC restriction of T cell receptors. *Nat. Rev. Immunol.* 18: 467–478.
8. Gras, S., J. Chadderton, C. M. Del Campo, C. Farenc, F. Wiede, T. M. Josephs, X. Y. X. Sng, M. Mirams, K. A. Watson, T. Tiganis, et al. 2016. Reversed T cell receptor docking on a major histocompatibility class I complex limits involvement in the immune response. *Immunity* 45: 749–760.
9. Beringer, D. X., F. S. Kleijwegt, F. Wiede, A. R. van der Slik, K. L. Loh, J. Petersen, N. L. Dudek, G. Duinkerken, S. Laban, A. Joosten, et al. 2015. T cell receptor reversed polarity recognition of a self-antigen major histocompatibility complex. *Nat. Immunol.* 16: 1153–1161.
10. Sharon, E., L. V. Sibener, A. Battle, H. B. Fraser, K. C. Garcia, and J. K. Pritchard. 2016. Genetic variation in MHC proteins is associated with T cell receptor expression biases. *Nat. Genet.* 48: 995–1002.
11. Dash, P., A. J. Fiore-Gartland, T. Hertz, G. C. Wang, S. Sharma, A. Souquette, J. C. Crawford, E. B. Clemens, T. H. O. Nguyen, K. Kedzierska, et al. 2017. Quantifiable predictive features define epitope-specific T cell receptor repertoires. *Nature* 547: 89–93.
12. Glanville, J., H. Huang, A. Nau, O. Hatton, L. E. Wagar, F. Rubelt, X. Ji, A. Han, S. M. Krams, C. Pettus, et al. 2017. Identifying specificity groups in the T cell receptor repertoire. *Nature* 547: 94–98.
13. Robinson, J., J. A. Halliwell, J. D. Hayhurst, P. Flicek, P. Parham, and S. G. Marsh. 2015. The IPD and IMGT/HLA database: allele variant databases. *Nucleic Acids Res.* 43(D1): D423–D431.
14. Gras, S., I. Van Rhijn, A. Shahine, T. Y. Cheng, M. Bhati, L. L. Tan, H. Halim, K. D. Tuttle, L. Gapin, J. Le Nours, et al. 2016. T cell receptor recognition of CD1b presenting a mycobacterial glycolipid. *Nat. Commun.* 7: 13257.
15. Van Rhijn, I., A. Kasmar, A. de Jong, S. Gras, M. Bhati, M. E. Doorenspleet, N. de Vries, D. I. Godfrey, J. D. Altman, W. de Jager, et al. 2013. A conserved human T cell population targets mycobacterial antigens presented by CD1b. *Nat. Immunol.* 14: 706–713.
16. Corbett, A. J., S. B. Eckle, R. W. Birkinshaw, L. Liu, O. Patel, J. Mahony, Z. Chen, R. Reantragoon, B. Meehan, H. Cao, et al. 2014. T-cell activation by transitory neo-antigens derived from distinct microbial pathways. *Nature* 509: 361–365.
17. Boudinot, P., S. Mondot, L. Jouneau, L. Teyton, M. P. Lefranc, and O. Lantz. 2016. Restricting nonclassical MHC genes coevolve with TRAV genes used by innate-like T cells in mammals. *Proc. Natl. Acad. Sci. USA* 113: E2983–E2992.
18. Turner, S. J., P. C. Doherty, J. McCluskey, and J. Rossjohn. 2006. Structural determinants of T-cell receptor bias in immunity. *Nat. Rev. Immunol.* 6: 883–894.
19. Grant, E. P., M. Degano, J. P. Rosat, S. Stenger, R. L. Modlin, I. A. Wilson, S. A. Porcelli, and M. B. Brenner. 1999. Molecular recognition of lipid antigens by T cell receptors. *J. Exp. Med.* 189: 195–205.
20. Cardell, S., S. Tangri, S. Chan, M. Kronenberg, C. Benoist, and D. Mathis. 1995. CD1-restricted CD4+ T cells in major histocompatibility complex class II-deficient mice. *J. Exp. Med.* 182: 993–1004.
21. Behar, S. M., T. A. Podrebarac, C. J. Roy, C. R. Wang, and M. B. Brenner. 1999. Diverse TCRs recognize murine CD1. *J. Immunol.* 162: 161–167.
22. Makowska, A., T. Kawano, M. Taniguchi, and S. Cardell. 2000. Differences in the ligand specificity between CD1d-restricted T cells with limited and diverse T-cell receptor repertoire. *Scand. J. Immunol.* 52: 71–79.

23. Jahng, A., I. Maricic, C. Aguilera, S. Cardell, R. C. Halder, and V. Kumar. 2004. Prevention of autoimmunity by targeting a distinct, noninvariant CD1d-reactive T cell population reactive to sulfatide. *J. Exp. Med.* 199: 947–957.

24. Van Rhijn, I., D. C. Young, J. S. Im, S. B. Levery, P. A. Illarionov, G. S. Besra, S. A. Porcelli, J. Gumperz, T. Y. Cheng, and D. B. Moody. 2004. CD1d-restricted T cell activation by nonlipidic small molecules. *Proc. Natl. Acad. Sci. USA* 101: 13578–13583.

25. Chiu, Y. H., J. Jayawardena, A. Weiss, D. Lee, S. H. Park, A. Dautry-Varsat, and A. Bendelac. 1999. Distinct subsets of CD1-restricted T cells recognize self-antigens loaded in different cellular compartments. *J. Exp. Med.* 189: 103–110.

26. Moody, D. B., B. B. Reinhold, M. R. Guy, E. M. Beckman, D. E. Frederique, S. T. Furlong, S. Ye, V. N. Reinhold, P. A. Sieling, R. L. Modlin, et al. 1997. Structural requirements for glycolipid antigen recognition by CD1b-restricted T cells. *Science* 278: 283–286.

27. Van Rhijn, I., N. A. Gherardin, A. Kasmar, W. de Jager, D. G. Pellicci, L. Kostenko, L. L. Tan, M. Bhati, S. Gras, D. I. Godfrey, et al. 2014. TCR bias and affinity define two compartments of the CD1b-glycolipid-specific T cell repertoire. *J. Immunol.* 192: 4054–4060.

28. Guo, T., M. Y. Koo, Y. Kagoya, M. Anczurowski, C. H. Wang, K. Saso, M. O. Butler, and N. Hirano. 2018. A subset of human autoreactive CD1c-restricted T cells preferentially expresses TRBV4-1⁺ TCRs. *J. Immunol.* 200: 500–511.

29. Aragão, D., J. Aishima, H. Cherukuvada, R. Clarken, M. Clift, N. P. Cowieson, D. J. Ericsson, C. L. Gee, S. Macedo, N. Mudie, et al. 2018. MX2: a high-flux undulator microfocus beamline serving both the chemical and macromolecular crystallography communities at the Australian Synchrotron. *J. Synchrotron Radiat.* 25: 885–891.

30. Winn, M. D., C. C. Ballard, K. D. Cowtan, E. J. Dodson, P. Emsley, P. R. Evans, R. M. Keegan, E. B. Krissinel, A. G. Leslie, A. McCoy, et al. 2011. Overview of the CCP4 suite and current developments. *Acta Crystallogr. D Biol. Crystallogr.* 67: 235–242.

31. Adams, P. D., P. V. Afonine, G. Bunkóczi, V. B. Chen, I. W. Davis, N. Echols, J. J. Headd, L. W. Hung, G. J. Kapral, R. W. Grosse-Kunstleve, et al. 2010. PHENIX: a comprehensive Python-based system for macromolecular structure solution. *Acta Crystallogr. D Biol. Crystallogr.* 66: 213–221.

32. Emsley, P., B. Lohkamp, W. G. Scott, and K. Cowtan. 2010. Features and development of Coot. *Acta Crystallogr. D Biol. Crystallogr.* 66: 486–501.

33. Van Rhijn, I., T. van Berlo, T. Hilmenyuk, T. Y. Cheng, B. J. Wolf, R. V. Tatituri, A. P. Uldrich, G. Napolitani, V. Cerundolo, J. D. Altman, et al. 2016. Human autoreactive T cells recognize CD1b and phospholipids. *Proc. Natl. Acad. Sci. USA* 113: 380–385.

34. Shahine, A., P. Reinink, J. F. Reijneveld, S. Gras, M. Holzheimer, T. Y. Cheng, A. J. Minnaard, J. D. Altman, S. Lenz, J. Prandi, et al. 2019. A T-cell receptor escape channel allows broad T-cell response to CD1b and membrane phospholipids. *Nat. Commun.* 10: 56.

35. Wang, G. C., P. Dash, J. A. McCullers, P. C. Doherty, and P. G. Thomas. 2012. T cell receptor αβ diversity inversely correlates with pathogen-specific antibody levels in human cytomegalovirus infection. *Sci. Transl. Med.* 4: 128ra42.

36. Layre, E., A. Collmann, M. Bastian, S. Mariotti, J. Czaplicki, J. Prandi, L. Mori, S. Stenger, G. De Libero, G. Puzo, and M. Gilleron. 2009. Mycolic acids constitute a scaffold for mycobacterial lipid antigens stimulating CD1-restricted T cells. *Chem. Biol.* 16: 82–92.

37. Beckman, E. M., S. A. Porcelli, C. T. Morita, S. M. Behar, S. T. Furlong, and M. B. Brenner. 1994. Recognition of a lipid antigen by CD1-restricted alpha beta+ T cells. *Nature* 372: 691–694.

38. Stenger, S., R. J. Mazzaccaro, K. Uyemura, S. Cho, P. F. Barnes, J. P. Rosat, A. Sette, M. B. Brenner, S. A. Porcelli, B. R. Bloom, and R. L. Modlin. 1997. Differential effects of cytolytic T cell subsets on intracellular infection. *Science* 276: 1684–1687.

39. Vincent, M. S., D. S. Leslie, J. E. Gumperz, X. Xiong, E. P. Grant, and M. B. Brenner. 2002. CD1-dependent dendritic cell instruction. *Nat. Immunol.* 3: 1163–1168.

40. Spada, F. M., E. P. Grant, P. J. Peters, M. Sugita, A. Melián, D. S. Leslie, H. K. Lee, E. van Donselaar, D. A. Hanson, A. M. Krensky, et al. 2000. Self-recognition of CD1 by gamma/delta T cells: implications for innate immunity. *J. Exp. Med.* 191: 937–948.

41. James, C. A., K. K. Q. Yu, M. Gilleron, J. Prandi, V. R. Yedulla, Z. Z. Moleda, E. Diamanti, M. Khan, V. K. Aggarwal, J. F. Reijneveld, et al. 2018. CD1b tetramers identify T cells that recognize natural and synthetic diacylated sulfoglycolipids from Mycobacterium tuberculosis. *Cell Chem. Biol.* 25: 392–402.e14.

42. Van Rhijn, I., S. K. Iwany, P. Fodran, T. Y. Cheng, L. Gapin, A. J. Minnaard, and D. B. Moody. 2017. CD1b-mycolic acid tetramers demonstrate T-cell fine specificity for mycobacterial lipid tails. *Eur. J. Immunol.* 47: 1525–1534.

43. Emerson, R., A. Sherwood, C. Desmarais, S. Malhotra, D. Phippard, and H. Robins. 2013. Estimating the ratio of CD4+ to CD8+ T cells using high-throughput sequence data. *J. Immunol. Methods* 391: 14–21.

44. Freeman, J. D., R. L. Warren, J. R. Webb, B. H. Nelson, and R. A. Holt. 2009. Profiling the T-cell receptor beta-chain repertoire by massively parallel sequencing. *Genome Res.* 19: 1817–1824.

45. Warren, R. L., J. D. Freeman, T. Zeng, G. Choe, S. Munro, R. Moore, J. R. Webb, and R. A. Holt. 2011. Exhaustive T-cell repertoire sequencing of human peripheral blood samples reveals signatures of antigen selection and a directly measured repertoire size of at least 1 million clonotypes. *Genome Res.* 21: 790–797.

46. Shahine, A., I. Van Rhijn, T. Y. Cheng, S. Iwany, S. Gras, D. B. Moody, and J. Rossjohn. 2017. A molecular basis of human T cell receptor autoreactivity toward self-phospholipids. *Sci. Immunol.* 2: eaao1384.

47. Garcia-Alles, L. F., A. Collmann, C. Versluis, B. Lindner, J. Guiard, L. Maveyraud, E. Huc, J. S. Im, S. Sansano, T. Brando, et al. 2011. Structural reorganization of the antigen-binding groove of human CD1b for presentation of mycobacterial sulfoglycolipids. *Proc. Natl. Acad. Sci. USA* 108: 17755–17760.

48. DeWitt, W. S., K. K. Q. Yu, D. B. Wilburn, A. Sherwood, M. Vignali, C. L. Day, T. J. Scriba, H. S. Robins, W. J. Swanson, R. O. Emerson, et al. 2018. A diverse lipid antigen-specific TCR repertoire is clonally expanded during active tuberculosis. *J. Immunol.* 201: 888–896.

49. Moody, D. B., M. R. Guy, E. Grant, T. Y. Cheng, M. B. Brenner, G. S. Besra, and S. A. Porcelli. 2000. CD1b-mediated T cell recognition of a glycolipid antigen generated from mycobacterial lipid and host carbohydrate during infection. *J. Exp. Med.* 192: 965–976.

50. Gadola, S. D., N. R. Zaccai, K. Harlos, D. Shepherd, J. C. Castro-Palomino, G. Ritter, R. R. Schmidt, E. Y. Jones, and V. Cerundolo. 2002. Structure of human CD1b with bound ligands at 2.3 A, a maze for alkyl chains. *Nat. Immunol.* 3: 721–726.

51. Relloso, M., T. Y. Cheng, J. S. Im, E. Parisini, C. Roura-Mir, C. DeBono, D. M. Zajonc, L. F. Murga, M. J. Ondrechen, I. A. Wilson, et al. 2008. pH-dependent interdomain tethers of CD1b regulate its antigen capture. *Immunity* 28: 774–786.

52. Patel, O., L. Kjer-Nielsen, J. Le Nours, S. B. Eckle, R. Birkinshaw, T. Beddoe, A. J. Corbett, L. Liu, J. J. Miles, B. Meehan, et al. 2013. Recognition of vitamin B metabolites by mucosal-associated invariant T cells. *Nat. Commun.* 4: 2142.

53. López-Sagaseta, J., C. L. Dulberger, J. E. Crooks, C. D. Parks, A. M. Luoma, A. McFedries, I. Van Rhijn, A. Saghatelian, and E. J. Adams. 2013. The molecular basis for mucosal-associated invariant T cell recognition of MR1 proteins. *Proc. Natl. Acad. Sci. USA* 110: E1771–E1778.

54. Borg, N. A., K. S. Wun, L. Kjer-Nielsen, M. C. Wilce, D. G. Pellicci, R. Koh, G. S. Besra, M. Bharadwaj, D. I. Godfrey, J. McCluskey, and J. Rossjohn. 2007. CD1d-lipid-antigen recognition by the semi-invariant NKT T-cell receptor. *Nature* 448: 44–49.

55. Grant, E. P., E. M. Beckman, S. M. Behar, M. Degano, D. Frederique, G. S. Besra, I. A. Wilson, S. A. Porcelli, S. T. Furlong, and M. B. Brenner. 2002. Fine specificity of TCR complementarity-determining region residues and lipid antigen hydrophilic moieties in the recognition of a CD1-lipid complex. *J. Immunol.* 168: 3933–3940.

56. Wun, K. S., J. F. Reijneveld, T. Y. Cheng, K. Ladell, A. P. Uldrich, J. Le Nours, K. L. Miners, J. E. McLaren, J. E. Grant, O. L. Haigh, et al. 2018. T cell autoreactivity directed toward CD1c itself rather than toward carried self lipids. *Nat. Immunol.* 19: 397–406.

57. Dascher, C. C., K. Hiromatsu, J. W. Naylor, P. P. Brauer, K. A. Brown, J. R. Storey, S. M. Behar, E. S. Kawasaki, S. A. Porcelli, M. B. Brenner, and K. P. LeClair. 1999. Conservation of a CD1 multigene family in the guinea pig. *J. Immunol.* 163: 5478–5488.

58. Dossa, R. G., D. C. Alperin, M. T. Hines, and S. A. Hines. 2014. The equine CD1 gene family is the largest and most diverse yet identified. *Immunogenetics* 66: 33–42.

59. Eguchi-Ogawa, T., T. Morozumi, M. Tanaka, H. Shinkai, N. Okumura, K. Suzuki, T. Awata, and H. Uenishi. 2007. Analysis of the genomic structure of the porcine CD1 gene cluster. *Genomics* 89: 248–261.

60. Hayes, S. M., and K. L. Knight. 2001. Group 1 CD1 genes in rabbit. *J. Immunol.* 166: 403–410.

61. Looringh van Beeck, F. A., D. M. Zajonc, P. F. Moore, Y. M. Schlotter, F. Broere, V. P. Rutten, T. Willemse, and I. Van Rhijn. 2008. Two canine CD1a proteins are differentially expressed in skin. *Immunogenetics* 60: 315–324.

62. Reinink, P., and I. Van Rhijn. 2016. Mammalian CD1 and MR1 genes. *Immunogenetics* 68: 515–523.

63. Van Rhijn, I., A. P. Koets, J. S. Im, D. Piebes, F. Reddington, G. S. Besra, S. A. Porcelli, W. van Eden, and V. P. Rutten. 2006. The bovine CD1 family contains group 1 CD1 proteins, but no functional CD1d. *J. Immunol.* 176: 4888–4893.

64. Bradbury, A., K. T. Belt, T. M. Neri, C. Milstein, and F. Calabi. 1988. Mouse CD1 is distinct from and co-exists with TL in the same thymus. *EMBO J.* 7: 3081–3086.

65. Bosc, N., and M. P. Lefranc. 2000. The mouse (*Mus musculus*) T cell receptor beta variable (TRBV), diversity (TRBD) and joining (TRBJ) genes. *Exp. Clin. Immunogenet.* 17: 216–228.

66. Koop, B. F., and L. Hood. 1994. Striking sequence similarity over almost 100 kilobases of human and mouse T-cell receptor DNA. *Nat. Genet.* 7: 48–53.

67. Larrouy-Maumus, G., E. Layre, S. Clark, J. Prandi, E. Rayner, A. Williams, G. de Libero, G. Puzo, and M. Gilleron. 2017. Protective efficacy of a lipid antigen vaccine in a guinea pig model of tuberculosis. *Vaccine* 35: 1395–1402.